Controllable Synthesis of Metal-Organic Frameworks Based on Anthracene Ligands for High Sensitivity Fluorescence Sensing of Fe^{3+}, $Cr_2O_7^{2-}$ and TNP

Jiao Li,[a] Jingfang Tian,[b] Haihuan Yu,[a] Mingyue Fan,[b] Xiao Li,[b*] Fangbin Liu,[b*], Jing Sun,[b] and Zhongmin Su[b*]

[a]School of Materials science and Engineering, Changchun University of Science and Technology, Changchun 130022, People's Republic of China.

[b]School of Chemical and Environmental Engineering, Jilin Provincial Science and Technology Innovation Centre of Optical Materials and Chemistry, Changchun University of Science and Technology, Changchun, 130022, People's Republic of China.

E-mail: lix@cust.edu.cn, zmsu@nenu.edu.cn.

Experimental Section

Materials and Characterization

All reagents are AR grade and commercially available. The ligand of 1-(9-(1H-1,2,4-triazol-1-yl) anthracen-10-yl)-1H-1,2,4-triazole (tatrz) is synthesized according to the literature [1]. Powder X-Ray diffraction (PXRD) patterns were obtained on a Siemens D5005 automated diffractometer with Cu Ka (1= 1.5418 Å) and range of 2θ was 5-40°. Infrared spectra were achieved on a Nicolet 380 FT-IR spectrophotometer (4000-400 cm^{-1}) by KBr pellets. UV-vis spectrums were collected on U-3010 spectrophotometer with the scan rang of 400-700 nm. Thermogravimetric analysis (TGA) was performed under nitrogen atmosphere at heating temperature of 25-800 ℃ (Perkin-Elmer FLS-920 analyzer). Fluorescence signals are collected on RF6000 spectrophotometer with the

emission range of 400-650 nm.

Synthesis of [Cd(tatrz)(1,4-BDC)] (CUST-601)

$Cd(NO_3)_2·4H_2O$ (0.060 g, 0.20 mmol), 1,4-BDC (0.020 g, 0.12 mmol), tatrz (0.018 g, 0.06 mmol) and DMF-methanol-water ($V_{2:2:4}$, 8 mL) are mixed and stirred for 30 min, and then sealed in a Teflon-lined stainless steel autoclave. The mixture was contained at 100 ℃ for 3 days, and refrigerated to room temperature naturally. Yellow crystals were collected in a 46% yield based on $Cd(NO_3)_2·4H_2O$. Anal. Calcd for $C_{26}H_{16}CdN_6O_4$ (M_r = 588.96): C, 53.06 %; H, 2.72 %; N, 14.28 %. Found: C, 52.41 %; H, 2.13 %; N, 14.05 %. IR data (KBr, cm^{-1}) (Figure S1): 3598(w), 3158 (w), 3103 (w), 2357 (w), 1569 (s),1499 (w),1443 (w), 1366 (s), 1255 (w), 1165 (w), 1129 (s), 1025 (m), 1004 (m), 969 (m), 928 (m), 886 (w), 809 (w), 774 (s), 760 (s), 649 (m), 551 (w), 495 (w).

Synthesis of $[Cd(tatrz)_{0.5}(1,3\text{-}BDC)CH_3CH_2OH]$ (CUST-602)

The synthesis of **CUST-602** was similar to **CUST-601** except that 1,3-BDC was instead of 1,4-BDC. Briefly, $Cd(NO_3)_2·4H_2O$ (0.060 g, 0.20 mmol), 1,3-BDC (0.020 g, 0.12 mmol), tatrz (0.018 g, 0.06 mmol) and DMF-methanol-water ($V_{2:2:4}$, 8 mL) are mixed and stirred for 30 min, and then sealed in a Teflon-lined stainless steel autoclave. The mixture was contained at 100 ℃ for 3 days, and refrigerated to room temperature naturally. Yellow crystals were collected in a 49% yield based on $Cd(NO_3)_2·4H_2O$. Anal. Calcd for $C_{19}H_{15}CdN_3O_5$ (Mr = 477.74): C, 47.72 %; H, 3.14 %; N, 8.79 %. Found: C, 46.61 %; H, 3.03 %; N, 8.26 %. IR data (KBr, cm^{-1}) (Figure S1): 3431 (w), 3117 (w), 2364 (w), 1611 (w), 1541 (s),1443 (w),1261 (w), 1214 w), 1171 (m), 1116 (m), 1080 (w), 1046 (m), 1025 (m), 976 (m), 928 (m), 907 (w), 843 (w), 781 (s), 746

(s), 718 (s), 655 (m), 557 (w), 509 (w).

Synthesis of [Cd(tatrz)(1,3,5-BTC)] (CUST-603)

The synthesis of CUST-603 was similar to **CUST-601** except that 1,3,5-BTC was instead of 1,4-BDC. $Cd(NO_3)_2 \cdot 4H_2O$ (0.060 g, 0.20 mmol), 1,3,5-BTC (0.025 g, 0.12 mmol), tatrz (0.018 g, 0.06 mmol) and DMF-methanol-water ($V_{2:2:4}$, 8 mL) are mixed and stirred for 30 min, and then sealed in a Teflon-lined stainless steel autoclave. The mixture was contained at 100 ℃ for 3 days, and refrigerated to room temperature naturally. Yellow crystals were collected in a 53% yield based on $Cd(NO_3)_2 \cdot 4H_2O$. Anal. Calcd for $C_{27}H_{15}Cd_2N_6O_6$ (*M*r = 631.85): C, 51.28 %; H, 2.37 %; N, 13.29%. Found: C, 52.45 %; H, 2.13 %; N, 13.08 %. IR data (KBr, cm^{-1}) (Figure S1): 3124 (w), 2350 (w),1722 (w),1261 (s), 1624 (s), 1548 (s), 1443 (m), 1353 (s), 1206 (w), 1123 (m), 1025 (m), 983 (m), 934 (s), 879 (w), 781 (s), 732 (s), 655 (m), 523 (w), 453 (w).

Synthesis of $[Cd_3(tatrz)_2(1,3,5\text{-}BTC)_2 \cdot 2H_2O]$ (CUST-604)

The synthesis of CUST-604 was similar to **CUST-603** except that 1,3,5-BTC (0.010 g, 0.035 mmol) and tatrz (0.030 g, 0.096 mmol) was instead of 1,3,5-BTC (0.020 g, 0.12 mmol), tatrz (0.018 g, 0.06 mmol). Yellow crystals were collected in a 45% yield based on $Cd(NO_3)_2 \cdot 4H_2O$. Anal. Calcd for $C_{54}H_{32}Cd_3N_{12}O_{14}$ (*M*r = 1410.11): C, 45.95 %; H, 2.27 %; N, 11.91 %. Found: C, 45.22 %; H, 2.04 %; N, 11.59 %. IR data (KBr, cm^{-1}) (Figure S1): 3493 (w), 2343 (w),1715 (w), 1624 (s), 1548 (s), 1443 (m), 1374 (s), 1199 (w), 1123 (m), 1010 (m), 983 (m), 920 (s), 767 (w), 738 (s), 711 (s), 655 (m), 530 (w), 453 (w).

Synthesis of $[Cd_3(tatrz)(BTB)_2 \cdot 2DMA]$ (CUST-605)

The synthesis of **CUST-605** was similar to **CUST-601** except that BTB and DMA-methanol ($V_{4:4}$, 8 mL) was instead of 1,4-BDC and DMF-methanol-water ($V_{2:2:4}$, 8 mL), respectively. Concretely, $Cd(NO_3)_2 \cdot 4H_2O$ (0.060 g, 0.20 mmol), BTB (0.052 g, 0.12 mmol), tatrz (0.018 g, 0.06 mmol) and DMF-methanol ($V_{4:4}$, 8 mL) are mixed and stirred for 30 min, and then sealed in a Teflon-lined stainless steel autoclave. The mixture was contained at 100 ℃ for 3 days, and refrigerated to room temperature naturally. Yellow crystals were collected in a 58% yield based on $Cd(NO_3)_2 \cdot 4H_2O$. Anal. Calcd for $C_{82}H_{62}Cd_3N_6O_{14}$ (*M*r = 1696.57): C, 57.99 %; H, 3.65 %; N, 4.95 %. Found: C, 58.36 %; H, 3.79 %; N, 4.28 %. IR data (KBr, cm^{-1}) (Figure S1): 3117 (w), 3033 (w), 2942 (w), 2357 (w),1645 (w), 1590 (w), 1506 (s), 1408 (vs), 1255 (s), 1199 (w), 1123 (m), 1018 (m), 920 (m), 871 (s), 788 (vs), 718 (s), 662 (m), 593 (w), 481 (m). IR spectra of CUST-601 -CUST-605 all show the characteristic peaks of tatrz ligand and corresponding carboxylate ligands, which exhibits the peaks ranges from 3000-3700 cm^{-1}corresponds to the stretching vibrations O-H and N-H bonds. The bands at 600-900 cm^{-1} could be attributed to benzene rings and anthracene.

X-ray Crystallography

All crystal diffraction data of **CUST-601~605** are collected by using the Bruker D8 VENTURE diffractometer at 25 ℃ with graphite monochromatic Mo Kα radiation (λ = 0.71073Å). The analysis of crystal data via using SHELXL-97 crystallography software. All the data was refined is based on full matrix least square method [2-4]. The refinement of non-hydrogen atoms by anisotropic temperature parameters.

Fluorescence detection

Firstly, solid state fluorescence detection was performed on the synthesized crystal to

determine the excitation emission wavelength. Secondly, a variety of solvent selectivity test was carried out on the crystal, and a stable organic solvent with a small amount of quenching was selected as the solvent of the whole system. Subsequently, a variety of metal ions and nitro explosives were selectively tested. Finally, the analyte was quantitatively detected.

Table S1. Crystallographic data and structural refinements for CUST-601 ~ 605.

No.	CUST-601	CUST-602	CUST-603	CUST-604	CUST-605
Empirical formula	$C_{26}H_{16}CdN_6O_4$	$C_{19}H_{15}CdN_3O_5$	$C_{27}H_{15}CdN_6O_6$	$C_{54}H_{32}Cd_3N_{12}O_{14}$	$C_{82}H_{62}Cd_3N_6O_{14}$
Formula weight	588.85	477.74	631.85	1410.11	1696.57
Temperature/K	295.00	273.15	298.00	295.05	295.55
Crystal system	triclinic	triclinic	triclinic	triclinic	triclinic
Space group	P-1	P-1	P-1	P-1	P-1
a/Å	4.9557(13)	8.3960(4)	10.2464(6)	9.7353(9)	13.0979(12)
b/Å	9.739(2)	10.0583(5)	10.3001(6)	9.8632(9)	14.0777(14)
c/Å	12.592(3)	12.1724(6)	13.0473(8)	15.9426(15)	14.1553(13)
α/°	76.452(10)	105.5090(10)	88.032(3)	91.717(4)	74.055(4)
β/°	88.966(11)	104.474(2)	72.021(3)	103.102(5)	75.896(4)
γ/°	78.322(10)	107.821(2)	71.701(2)	117.478(4)	78.831(4)
Volume/Å^3	578.3 (2)	879.16(8)	1240.54(13)	1306.6(2)	2411.4(4)
Z	1	2	2	1	1
Goodness-of-fit on F^2	1.097	1.096	1.043	1.064	1.040
Final R indexes [I>=2σ (I)]	R_1 = 0.0184, wR_2 = 0.0465	R_1 = 0.0306, wR_2 = 0.0841	R_1 = 0.0235, wR_2 = 0.0548	R_1 = 0.0341, wR_2 = 0.0688	R_1 = 0.0372, wR_2 = 0.0941
Final R indexes [all data]	R_1 = 0.0186, wR_2 = 0.0466	R_1 = 0.0310, wR_2 = 0.0844	R_1 = 0.0288, wR_2 = 0.0574	R_1 = 0.0550, wR_2 = 0.0752	R_1 = 0.0533, wR_2 = 0.1020
ρ_{cal}cg/cm^3	1.691	1.805	1.692	1.792	1.168
μ/mm^{-1}	0.992	10.295	0.937	1.291	0.710
F (000)	294.0	476.0	630.0	696.0	854.0
Radiation	MoKα (λ = 0.71073)	CuKα (λ = 1.54178)	MoKα (λ = 0.71073)	MoKα (λ = 0.71073)	MoKα (λ = 0.71073)
Index ranges	-5 ≤ h ≤ 5, -11 ≤ k ≤ 11, -14 ≤ l ≤ 14	-9 ≤ h ≤ 9, -11 ≤ k ≤ 11, -14 ≤ l ≤ 14	-12 ≤ h ≤ 12, -12 ≤ k ≤ 12, -15 ≤ l ≤ 15	-11 ≤ h ≤ 11, -11 ≤ k ≤ 11, -18 ≤ l ≤ 18	-15 ≤ h ≤ 15, -16 ≤ k ≤ 16, -16 ≤ l ≤ 16
Reflections collected	11522	26585	24988	28444	65905
Independent reflections	2034 [Rint = 0.0403, Rsigma = 0.0259]	3087 [R_{int} = 0.0414, R_{sigma} = 0.0223]	4412 [R_{int}= 0.0355, R_{sigma}= 0.0228]	4606 [Rint = 0.0754, Rsigma = 0.0459]	8532 [Rint = 0.0682, Rsigma = 0.0356]
Data/restraints/parameters	2034/0/169	3087/22/254	4412/3/362	4606/0/376	8532/1/478
2θ range for data collection/°	25.139	9.956 to 133.318	5.362 to 50.186	4.712 to 50.084	5.672 to 50.226
Largest diff. peak/hole / e Å^{-3}	0.33/-0.58	0.60/-1.70	0.83/-0.88	0.60/-0.52	1.22/-0.51

Table S2. Bond distances (Å) for CUST-601.

CUST-601	
Bond	**Distance (Å)**
Cd(1)-O(2)#1	2.3383(14)
Cd(1)-O(2)#2	2.3383(14)
Cd(1)-O(3)#3	2.2626(14)
Cd(1)-O(3)	2.2625(14)
Cd(1)-N(4)	2.3293(16)
Cd(1)-N(4)#3	2.3293(16)
CUST-601: [1]1+X,+Y,+Z; [2]-X,2-Y,1-Z; [3]1-X,2-Y,1-Z; [4]-X,1-Y,1-Z; [5]1-X,1-Y,2-Z	

Table S3. Bond distances (Å) for CUST-602.

CUST-602	
Bond	**Distance (Å)**
Cd(1)-O(1)	2.252(3)
Cd(1)-O(1)#1	2.502(3)
Cd(1)-O(2)#2	2.371(3)
Cd(1)-O(3)#2	2.358(3)
Cd(1)-O(5)	2.332(3)
Cd(1)-N(1)	2.253(3)
CUST-602: [1]-X,1-Y,1-Z; [2]+X,1+Y,+Z; [3]2-X,2-Y,2-Z	

Table S4. Bond distances (Å) for CUST-603.

CUST-603	
Bond	**Distance (Å)**
Cd(1)-O(6)#1	2.3490(16)
Cd(1)-O(2)#2	2.3703(17)
Cd(1)-O(1)#2	2.4047(17)
Cd(1)-N(4)	2.245(2)
Cd(1)-N(3)	2.336(2)
CUST-603: [1]1-X,1-Y,-Z; [2]1+X,+Y,+Z; [3]1-X,-Y,1-Z; [4]-X,2-Y,1-Z	

Table S5. Bond distances (Å) for CUST-604.

CUST-604	
Bond	**Distance (Å)**
Cd(1)-O(3)	2.164(3)
Cd(1)-O(3)#1	2.164(3)
Cd(1)-O(4)#2	2.301(3)
Cd(1)-O(4)#3	2.301(3)
Cd(1)-O(6)#4	2.469(3)
Cd(1)-O(6)#5	2.469(3)
Cd(2)-O(4)#6	2.301(3)
Cd(2)-O(5)#7	2.231(3)

Cd(2)-O(6)	2.416(3)
Cd(2)-O(8)	2.191(3)

CUST-604: [1]2-X,1-Y,-Z;[2]1-X,1-Y,-Z;[3]1+X,+Y,+Z;[4]1+X,1+Y,+Z;[5]1-X,-Y,-Z;[6]+X,-1+Y,+Z;[7]-1+X,-1+Y,+Z

Table S6. Bond distances (Å) for CUST-605.

CUST-605	
Bond	**Distance (Å)**
Cd(1)-O(1)#1	2.244(3)
Cd(1)-O(1)	2.244(3)
Cd(1)-O(2)#2	2.405(3)
Cd(1)-O(2)#3	2.405(3)
Cd(1)-N(1)	2.270(3)
Cd(1)-N(1)#1	2.270(3)
Cd(2)-O(2)#2	2.576(3)
Cd(2)-O(3)#2	2.234(3)
Cd(2)-O(4)#4	2.314(3)
Cd(2)-O(5)#4	2.331(3)
Cd(2)-O(6)	2.147(3)
Cd(2)-O(7)	2.298(4)

CUST-605: [1]1-X,-Y,1-Z; [2]1+X,+Y,-1+Z; [3]-X,-Y,2-Z; [4]1+X,-1+Y,+Z; [5]1-X,1-Y,1-Z

Table S7. Angles (°) for **CUST-601**.

CUST-601	
Bond	**Angle (°)**
O(2)#1-Cd(1)-O(2)#2	180.0
O(3)-Cd(1)-O(2)#2	92.24(5)
O(3)-Cd(1)-O(2)#1	87.76(5)
O(3)#3-Cd(1)-O(2)#1	92.24(5)
O(3)#3-Cd(1)-O(2)#2	87.76(5)
O(3)-Cd(1)-O(3)#3	180.0
O(3)#3-Cd(1)-N(4)	98.70(6)
O(3)#3-Cd(1)-N(4)#3	81.30(6)
O(3)-Cd(1)-N(4)	81.30(6)
O(3)-Cd(1)-N(4)#3	98.70(6)
N(4)-Cd(1)-O(2)#2	92.26(6)
N(4)-Cd(1)-O(2)#1	87.74(6)
N(4)#3-Cd(1)-O(2)#1	92.26(6)
N(4)#3-Cd(1)-O(2)#2	87.74(6)
N(4)-Cd(1)-N(4)#3	180.0

CUST-601: X,2-Y,1-Z;[2]1+X,+Y,+Z;[3]1-X,2-Y,1-Z;[4]-1+X,+Y,+Z;[5]-X,1-Y,1-Z;[6]1-X,1-Y,2-Z

Table S8. Angles (°) for **CUST-602**.

CUST-602	
Bond	**Angle (°)**
O(1)-Cd(1)-O(1)#1	78.38(9)
O(1)-Cd(1)-O(2)#2	138.58(9)
O(1)-Cd(1)-O(3)#2	84.71(9)
O(1)-Cd(1)-O(5)	109.59(12)
O(1)-Cd(1)-N(1)	118.52(10)
O(2)#2-Cd(1)-O(1)#1	88.21(9)
O(3)#2-Cd(1)-O(1)#1	85.92(10)
O(3)#2-Cd(1)-O(2)#2	55.11(10)
O(5)-Cd(1)-O(1)#1	172.00(11)
O(5)-Cd(1)-O(2)#2	86.48(12)
O(5)-Cd(1)-O(3)#2	95.92(12)
N(1)-Cd(1)-O(1)#1	81.51(10)
N(1)-Cd(1)-O(2)#2	97.50(11)
N(1)-Cd(1)-O(3)#2	150.29(10)
N(1)-Cd(1)-O(5)	93.25(12)
Cd(1)-O(1)-Cd(1)#1	101.62(9)
CUST-602: [1]-X,1-Y,1-Z; [2]+X,1+Y,+Z; [3]+X,-1+Y,+Z; [4]2-X,2-Y,2-Z	

Table S9. Angles (°) for **CUST-603**.

CUST-603	
Bond	**Angle (°)**
O(6)-Cd(1)-O(6)#1	78.47(6)
O(6)-Cd(1)-O(2)#2	147.12(6)
O(6)#1-Cd(1)-O(2)#2	95.80(6)
O(6)#1-Cd(1)-O(1)#2	88.94(6)
O(6)-Cd(1)-O(1)#2	92.32(6)
O(6)-Cd(1)-N(4)	123.27(7)
O(6)-Cd(1)-N(3)	93.93(7)
O(2)#2-Cd(1)-O(1)#2	54.99(6)
N(4)-Cd(1)-O(6)#1	96.73(7)
N(4)-Cd(1)-O(2)#2	89.43(7)
N(4)-Cd(1)-O(1)#2	144.40(7)
N(4)-Cd(1)-N(3)	94.79(8)
N(3)-Cd(1)-O(6)#1	168.38(7)
N(3)-Cd(1)-O(2)#2	85.80(7)
N(3)-Cd(1)-O(1)#2	82.54(8)
Cd(1)-O(6)-Cd(1)#1	101.53(6)
CUST-603: [1]1-X,1-Y,-Z;[2]1+X,+Y,+Z;[3]-1+X,+Y,+Z;[4]1-X,-Y,1-Z;[5]-X,2-Y,1-Z	

Table S10. Angles (°) for **CUST-604**.

CUST-604	
Bond	**Angle (°)**
O(3)-Cd(1)-O(3)#1	180.00(13)
O(3)#1-Cd(1)-O(4)#2	94.01(11)
O(3)-Cd(1)-O(4)#2	85.99(11)
O(3)#1-Cd(1)-O(4)#3	85.99(11)
O(3)-Cd(1)-O(4)#3	94.01(11)
O(3)#1-Cd(1)-O(6)#4	89.01(10)
O(3)-Cd(1)-O(6)#4	90.99(10)
O(3)-Cd(1)-O(6)#5	89.01(10)
O(3)#1-Cd(1)-O(6)#5	90.99(10)
O(4)#3-Cd(1)-O(4)#2	180.00(13)
O(4)#3-Cd(1)-O(6)#5	103.42(10)
O(4)#3-Cd(1)-O(6)#4	76.58(10)
O(4)#2-Cd(1)-O(6)#4	103.42(10)
O(4)#2-Cd(1)-O(6)#5	76.58(10)
O(6)#4-Cd(1)-O(6)#5	180.00(14)
O(4)#6-Cd(2)-O(6)	77.65(10)
O(5)#7-Cd(2)-O(4)#6	101.52(11)
O(5)#7-Cd(2)-O(6)	85.72(11)
O(8)-Cd(2)-O(4)#6	123.61(11)
O(8)-Cd(2)-O(5)#7	134.34(12)
O(8)-Cd(2)-O(6)	96.60(12)
Cd(2)#8-O(4)- Cd(1)#9	98.99(11)
CUST-604: [1]2-X,1-Y,-Z;[2]1+X,+Y,+Z;[3]1-X,1-Y,-Z; [4]1-X,-Y,-Z;[5]1+X,1+Y,+Z;[6]+X,-1+Y,+Z;[7]-1+X,-1+Y,+Z;[8]+X,1+Y,+Z;[9]-1+X,+Y,+Z	

Table S11. Angles (°) for **CUST-605**.

CUST-605	
Bond	**Angle (°)**
O1#1 Cd(1)-O(1)	180.0
O(1)-Cd(1)-O(2)#2	83.46(10)
O(1)#1-Cd(1)-O(2)#3	83.46(10)
O(1)#1-Cd(1)-O(2)#2	96.54(10)
O(1)-Cd(1)-O(2)#3	96.54(10)
O(1)#1-Cd(1)-N(1)	90.20(11)
O(1)#1-Cd(1)-N(1)#1	89.80(11)
O(1)-Cd(1)-N(1)#1	90.20(11)
O(1)-Cd(1)-N(1)	89.80(11)
O(2)#2-Cd(1)-N(2)#3	180.0 (14)
N(1)-Cd(1)-O(2)#3	92.32(11)
N(1)#1 -Cd(1)-O(2)#2	92.32(11)

N(1)-Cd(1)- O(2)#2	87.68(11)
N(1)#1-Cd(1)-O(2)#3	87.68(11)
N(1)-Cd(1)-N(1)#1	180.0
O(3)#2-Cd(2)-O(2)#2	53.44(9)
O(3)#2-Cd(2)-O(4)#4	91.20(13)
O(3)#3-Cd(2)-O(5)#4	125.03(12)
O(3)#2-Cd(2)-O(7)	84.55(14)
O(4)#4-Cd(2)-O(2)#2	94.16(10)
O(4)#4-Cd(2)-O(5)#4	55.52(10)
O(5)#4-Cd(2)-O(2)#2	149.10(11)
O(6)-Cd(2)-O(2)#2	91.59(12)
O(6)-Cd(2)-O(2)#3	132.99(15)
O(6)-Cd(2)-O(4)#4	125.38(15)
O(6)-Cd(2)-O(5)#4	101.27(14)
O(6)-Cd(2)-O(7)	91.99(15)
O(7)-Cd(2)-O(2)#2	121.35(15)
O(7)-Cd(2)-O(4)#4	129.45(15)
O(7)-Cd(2)-O(5)#4	86.73(15)
Cd(1)#5-O(2)-Cd(2)#5	116.48(10)

CUST-605: [1]1-X,-Y,1-Z; [2]1+X,+Y,-1+Z; [3]-X,-Y,2-Z; [4]1+X,-1+Y,+Z; [5]-1+X,+Y,1+Z; [6]-1+X,1+Y,+Z; [7]1-X,1-Y,1-Z

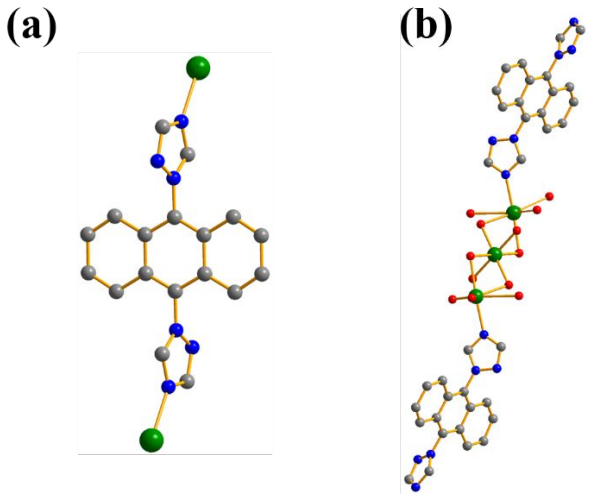

Figure S1. The coordination mode of tatrz.

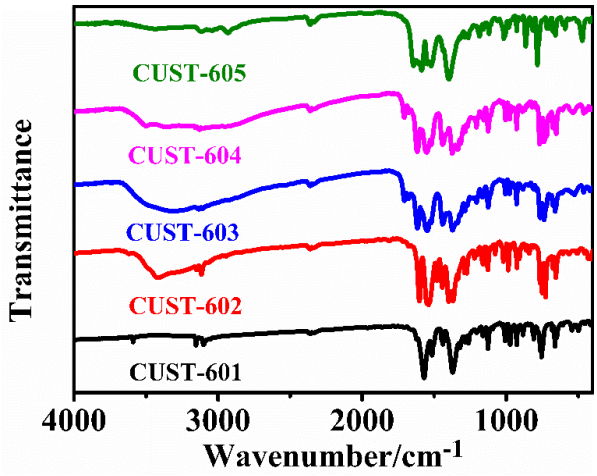

Figure S2. FTIR spectrum of five MOFs.

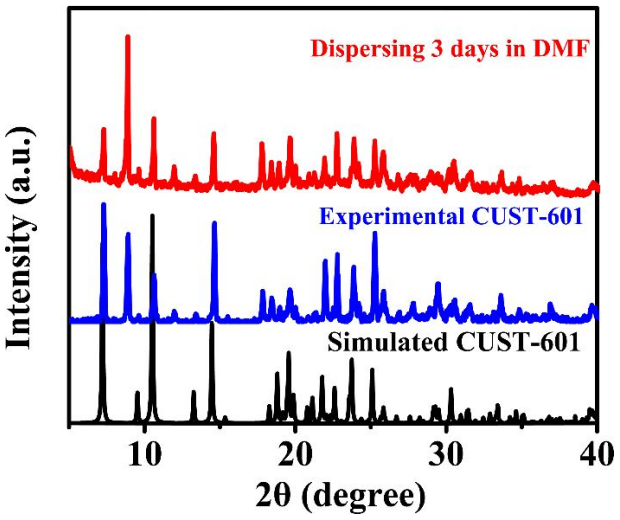

Figure S3. Powder X-ray diffraction patterns of **CUST-601**.

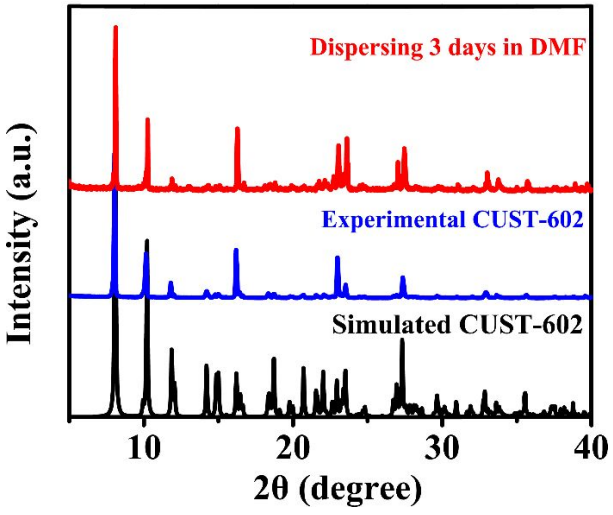

Figure S4. Powder X-ray diffraction patterns of CUST-602.

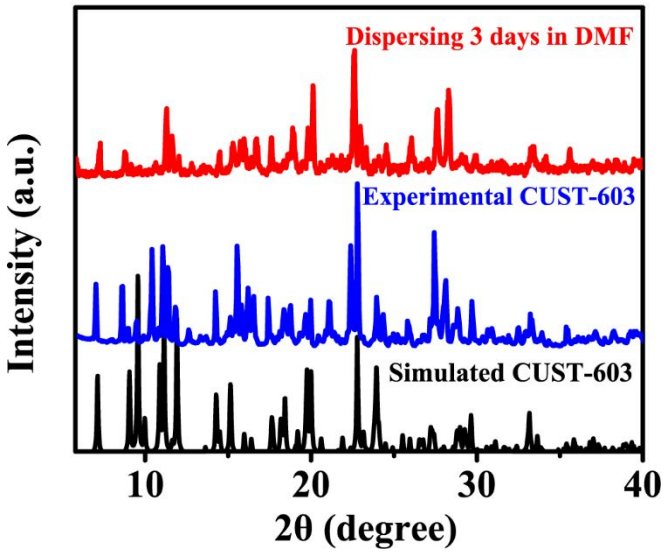

Figure S5. Powder X-ray diffraction patterns of CUST-603.

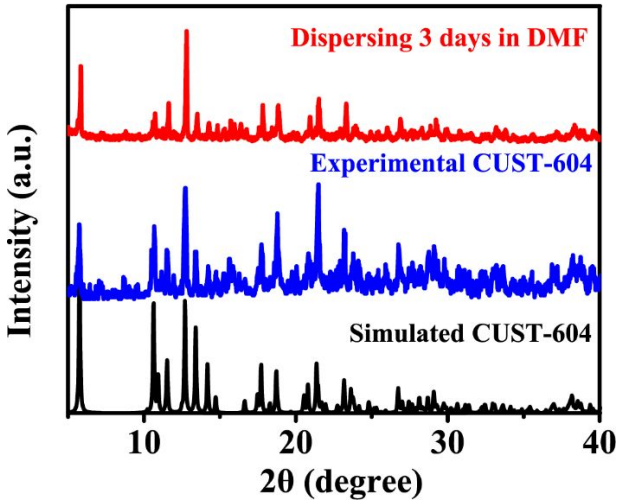

Figure S6. Powder X-ray diffraction patterns of CUST-604.

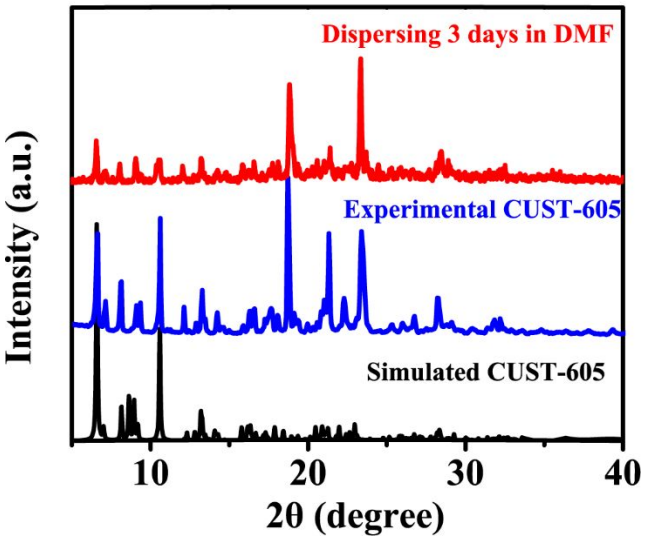

Figure S7. Powder X-ray diffraction patterns of **CUST-605**.

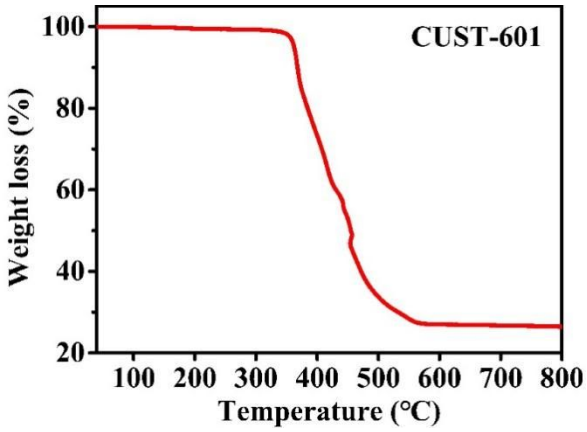

Figure S8. TG curves of CUST-601.

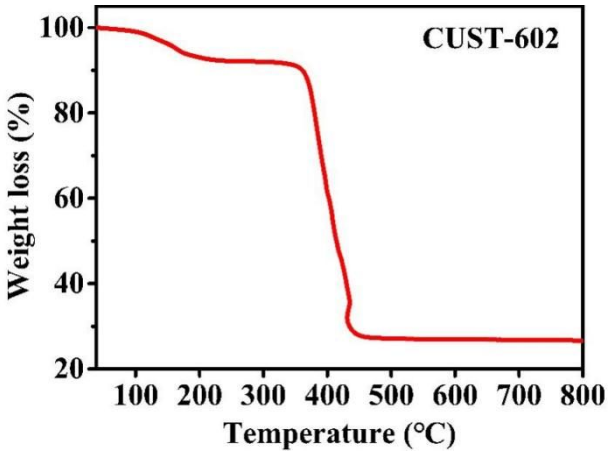

Figure S9. TG curves of CUST-602.

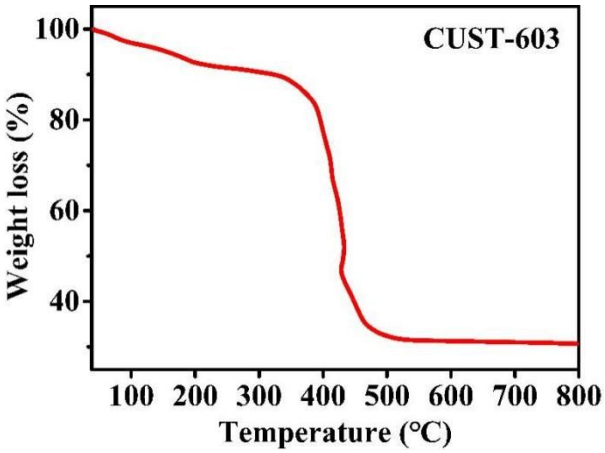

Figure S10. TG curves of CUST-603.

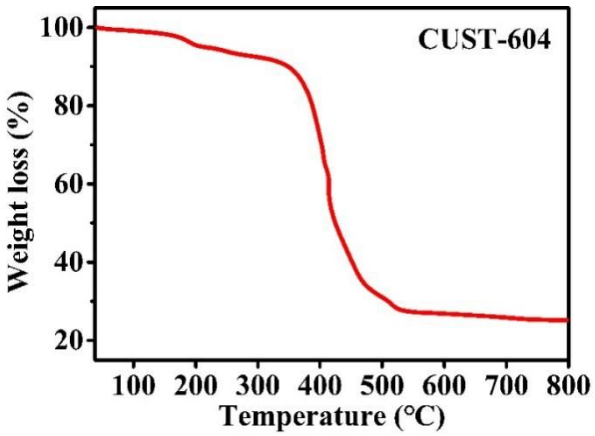

Figure S11. TG curves of CUST-604.

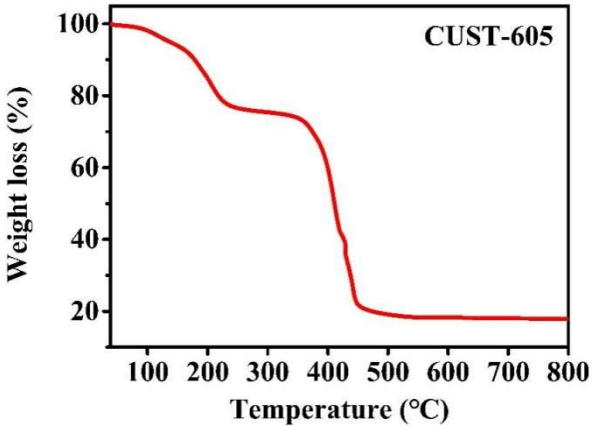

Figure S12. TG curves of CUST-605.

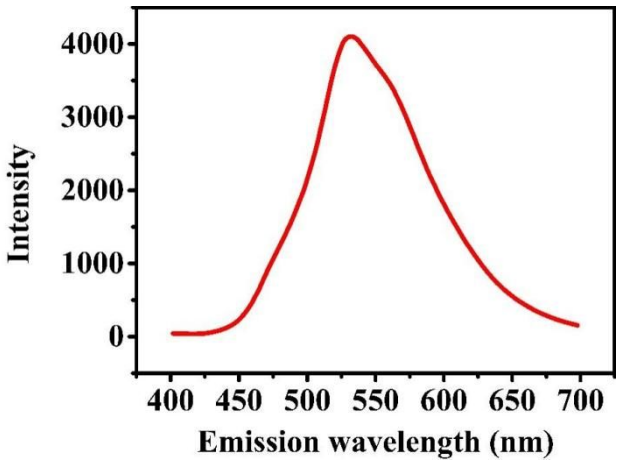

Figure S13. The solid-state Emission spectra of tatrz with the excitation wavelength of 380 nm at environment temperature.

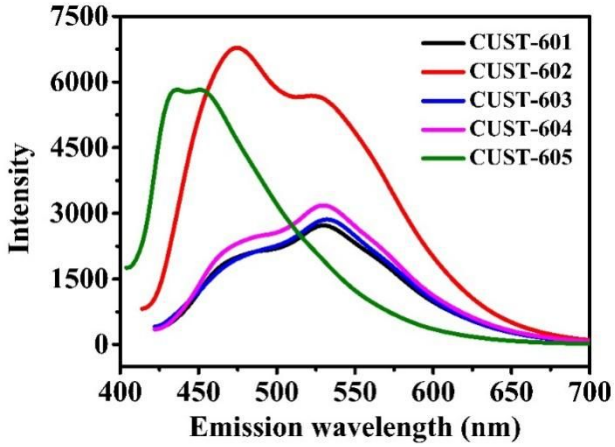

Figure S14. The solid-state Emission spectra of CUST-601~605 with the excitation wavelength of 374 ± 5 nm at environment temperature.

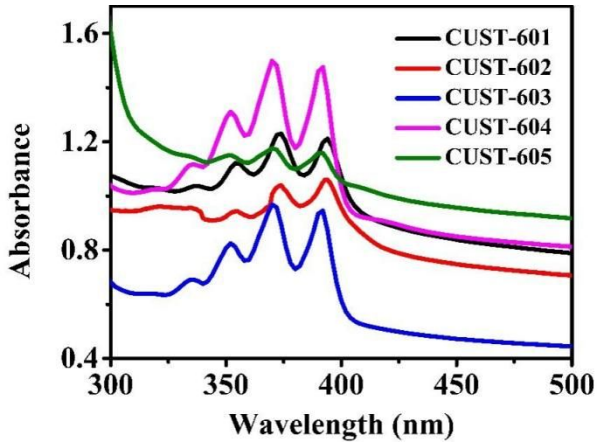

Figure S15. The UV-vis spectra of CUST-601~605.

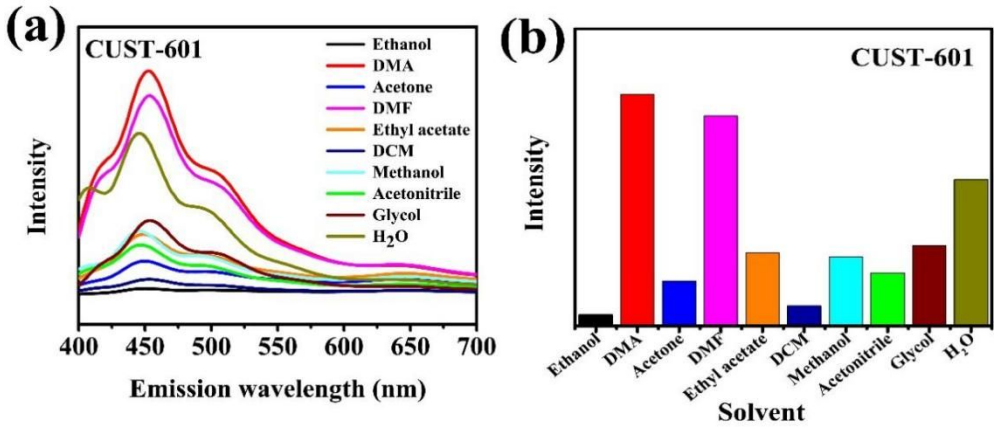

Figure S16. (a) Fluorescence spectrums and (b) contrast of fluorescence intensity of CUST-601 (λ_{ex} = 374 nm) with different solvents.

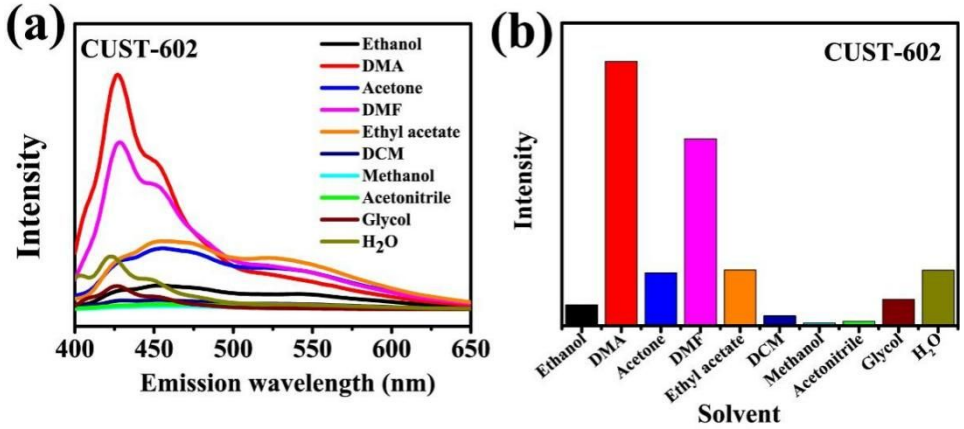

Figure S17. (a) Fluorescence spectrums and (b) contrast of fluorescence intensity of CUST-602 (λ_{ex} = 374 nm) with different solvents.

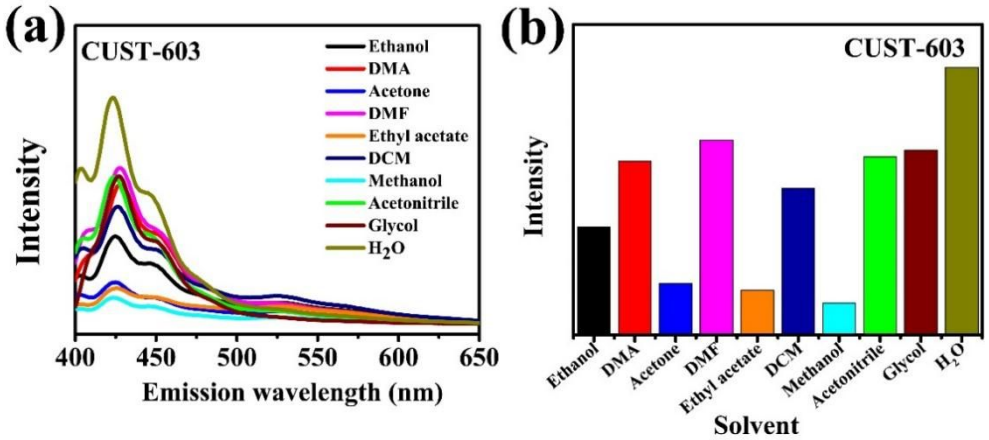

Figure S18. (a) Fluorescence spectrums and (b) contrast of fluorescence intensity of CUST-603 (λ_{ex} = 371 nm) with different solvents.

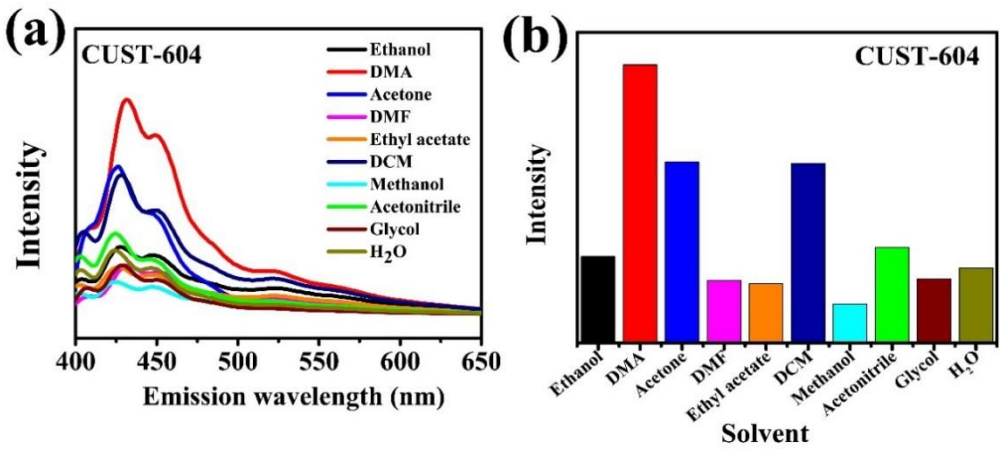

Figure S19. (a) Fluorescence spectrums and (b) contrast of fluorescence intensity of CUST-604 (λ_{ex} = 371 nm) with different solvents.

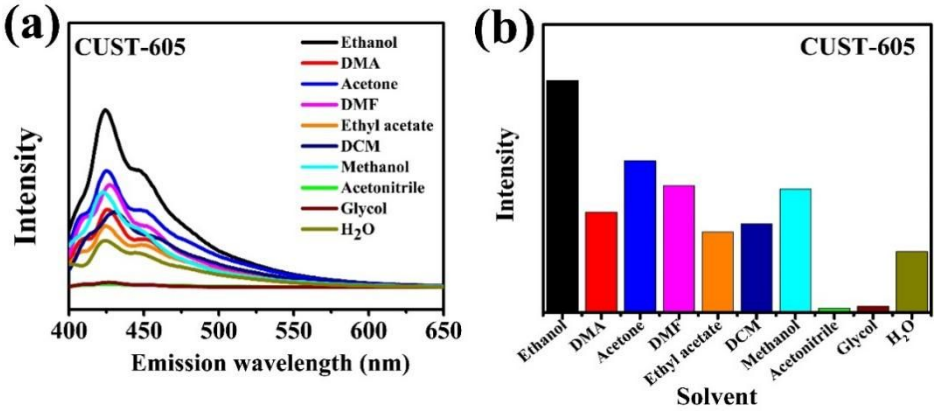

Figure S20. (a) Fluorescence spectrums and (b) contrast of fluorescence intensity of CUST-605 (λ_{ex} = 372 nm) with different solvents.

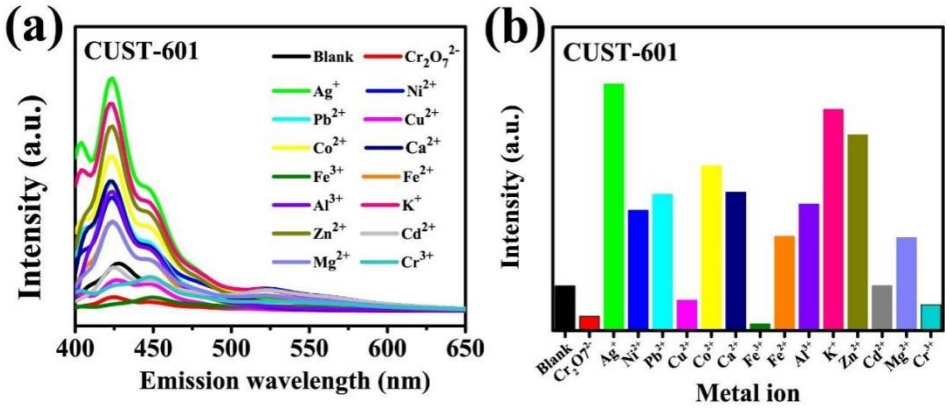

Figure S21. (a) Fluorescence spectrums and (b) contrast of fluorescence intensity of CUST-601 (λ_{ex} = 374 nm) with different metal ions.

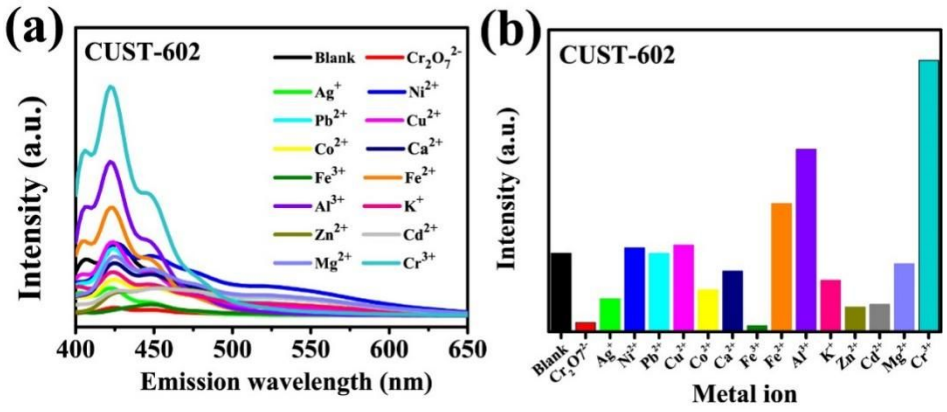

Figure S22. (a) Fluorescence spectrums and (b) contrast of fluorescence intensity of CUST-602 (λ_{ex} = 374 nm) with different metal ions.

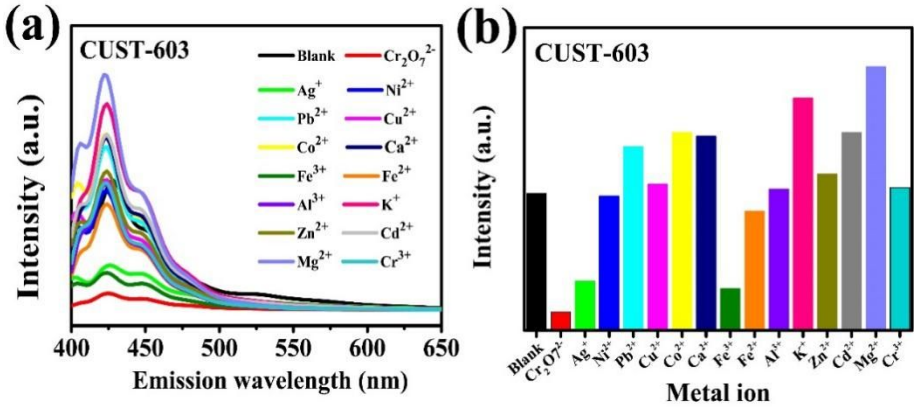

Figure S23. (a) Fluorescence spectrums and (b) contrast of fluorescence intensity of CUST-603 (λ_{ex} = 371 nm) with different metal ions.

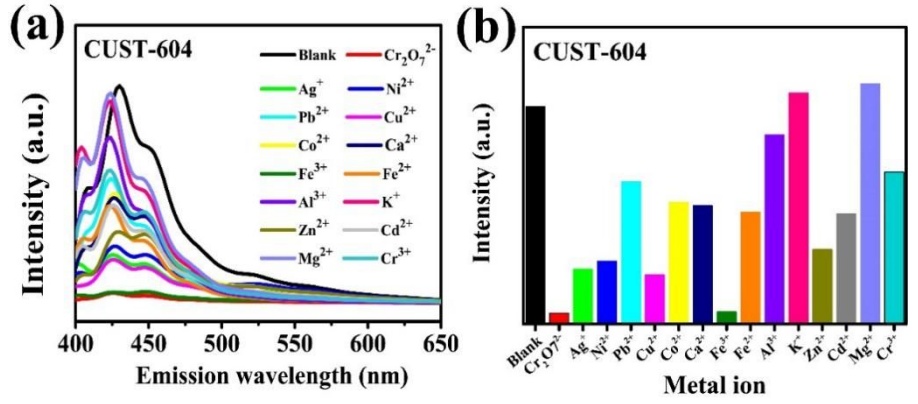

Figure S24. (a) Fluorescence spectrums and (b) contrast of fluorescence intensity of CUST-604 (λ_{ex} = 371 nm) with different metal ions.

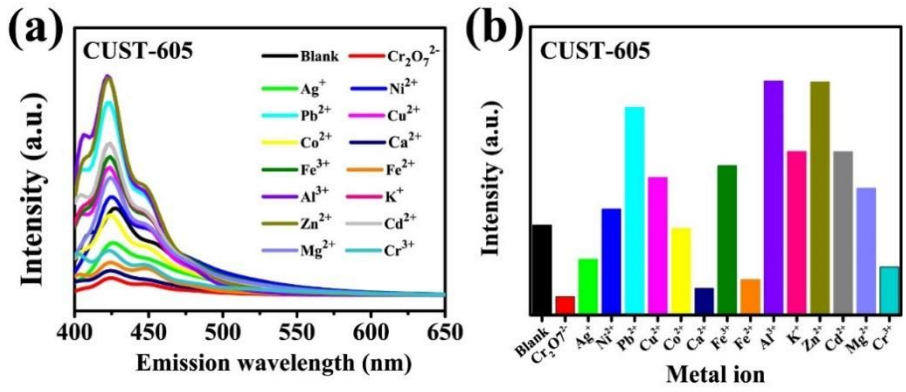

Figure S25. (a) Fluorescence spectrums and (b) contrast of fluorescence intensity of CUST-605 (λ_{ex} = 372 nm) with different metal ions.

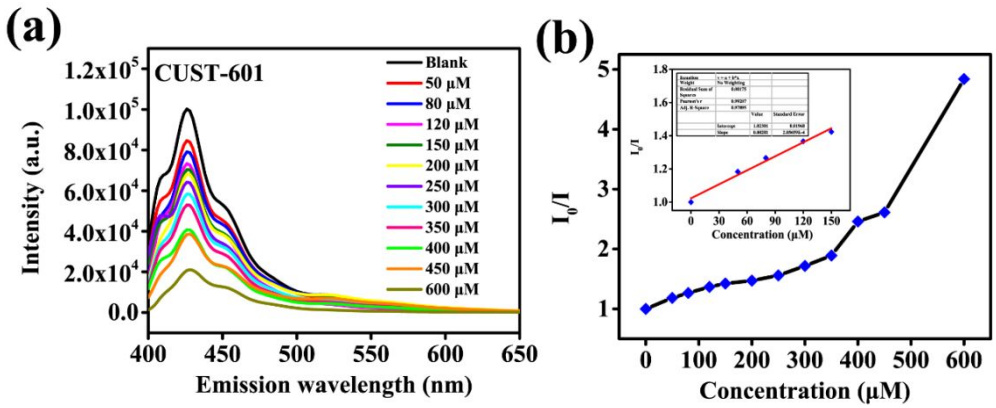

Figure S26. (a) Fluorescence spectrums of CUST-601 with increasing Fe^{3+} concentration. (b) S-V plot of CUST-601 with increasing Fe^{3+} concentration.

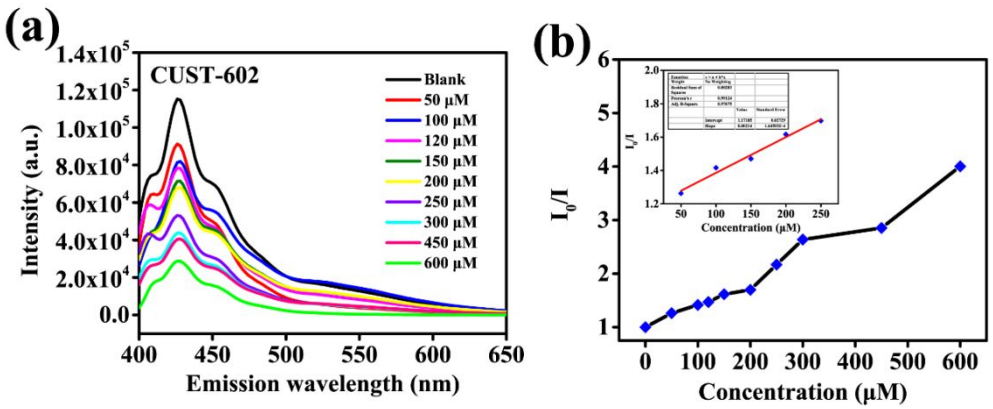

Figure S27. (a) Fluorescence spectrums of CUST-602 with increasing Fe^{3+} concentration. (b) S-V plot of CUST-602 with increasing Fe^{3+} concentration.

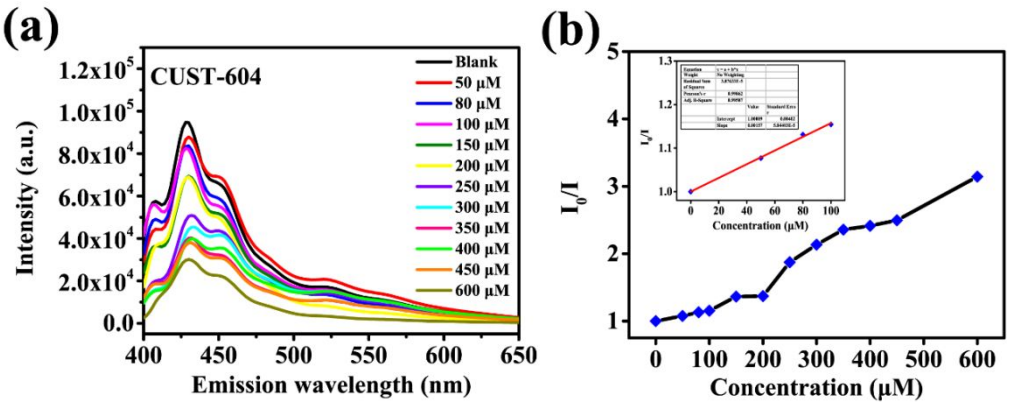

Figure S28. (a) Fluorescence spectrums of CUST-604 with increasing Fe^{3+} concentration. (b) S-V plot of CUST-604 with increasing Fe^{3+} concentration.

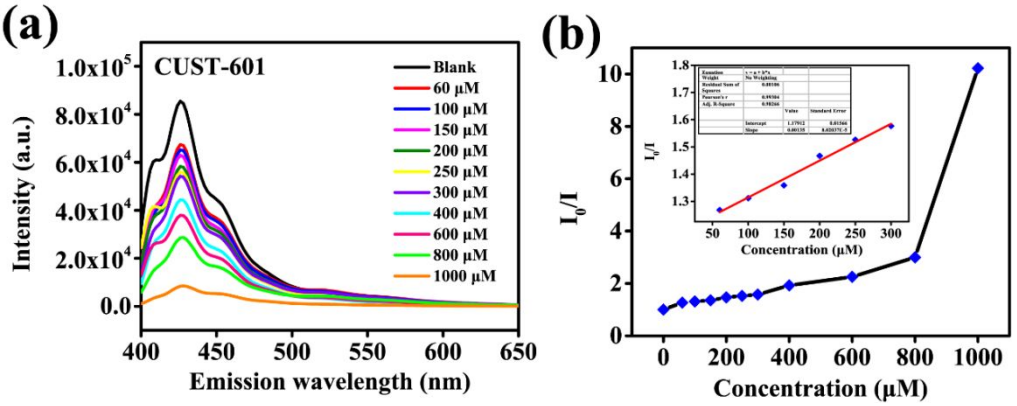

Figure S29. (a) Fluorescence spectrums of CUST-601 with increasing $Cr_2O_7^{2-}$ concentration. (b) S-V plot of CUST-601 with increasing $Cr_2O_7^{2-}$ concentration.

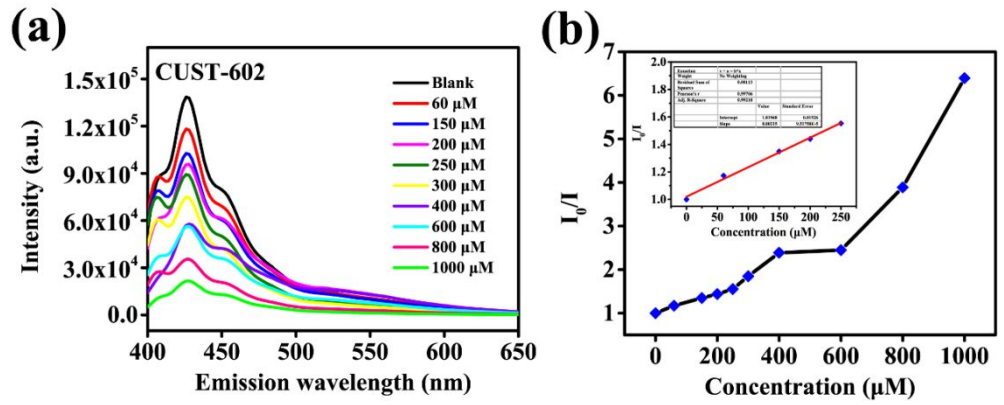

Figure S30. (a) Fluorescence spectrums of CUST-602 with increasing $Cr_2O_7^{2-}$ concentration. (b) S-V plot of CUST-602 with increasing $Cr_2O_7^{2-}$ concentration.

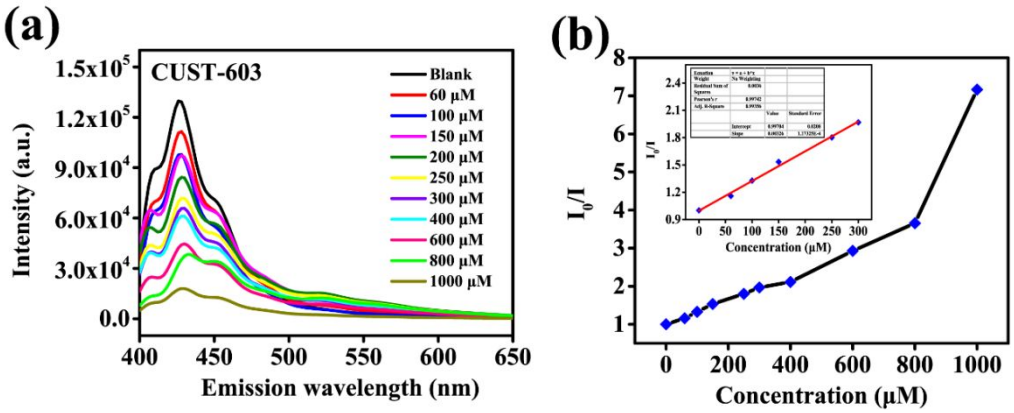

Figure S31. (a) Fluorescence spectrums of CUST-603 with increasing $Cr_2O_7^{2-}$ concentration. (b) S-V plot of CUST-603 with increasing $Cr_2O_7^{2-}$ concentration.

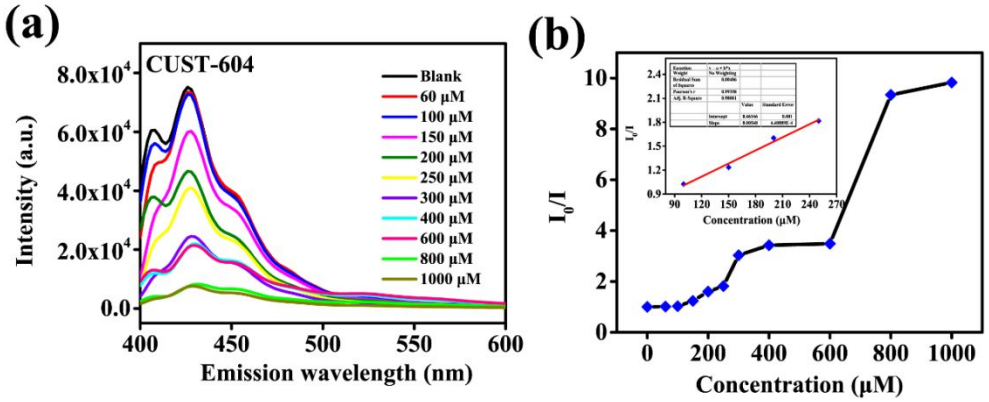

Figure S32. (a) Fluorescence spectrums of CUST-604 with increasing $Cr_2O_7^{2-}$ concentration. (b) S-V plot of CUST-604 with increasing $Cr_2O_7^{2-}$ concentration.

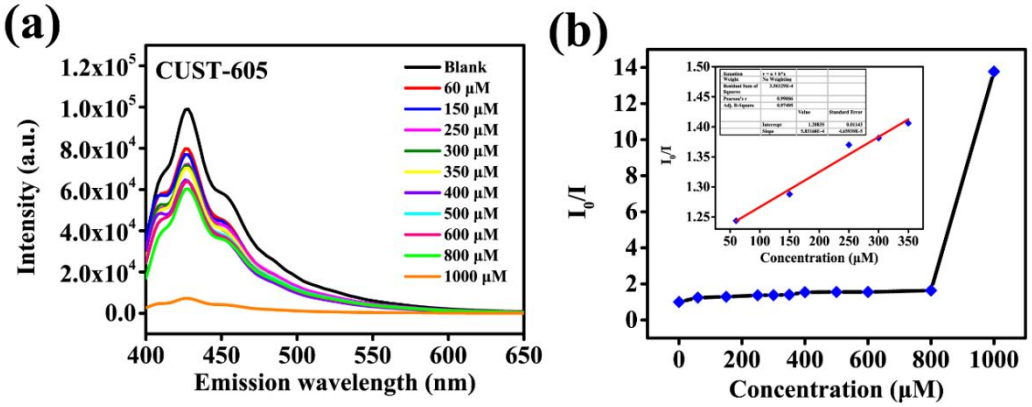

Figure S33. (a) Fluorescence spectrums of CUST-605 with increasing $Cr_2O_7^{2-}$ concentration. (b) S-V plot of CUST-605 with increasing $Cr_2O_7^{2-}$ concentration.

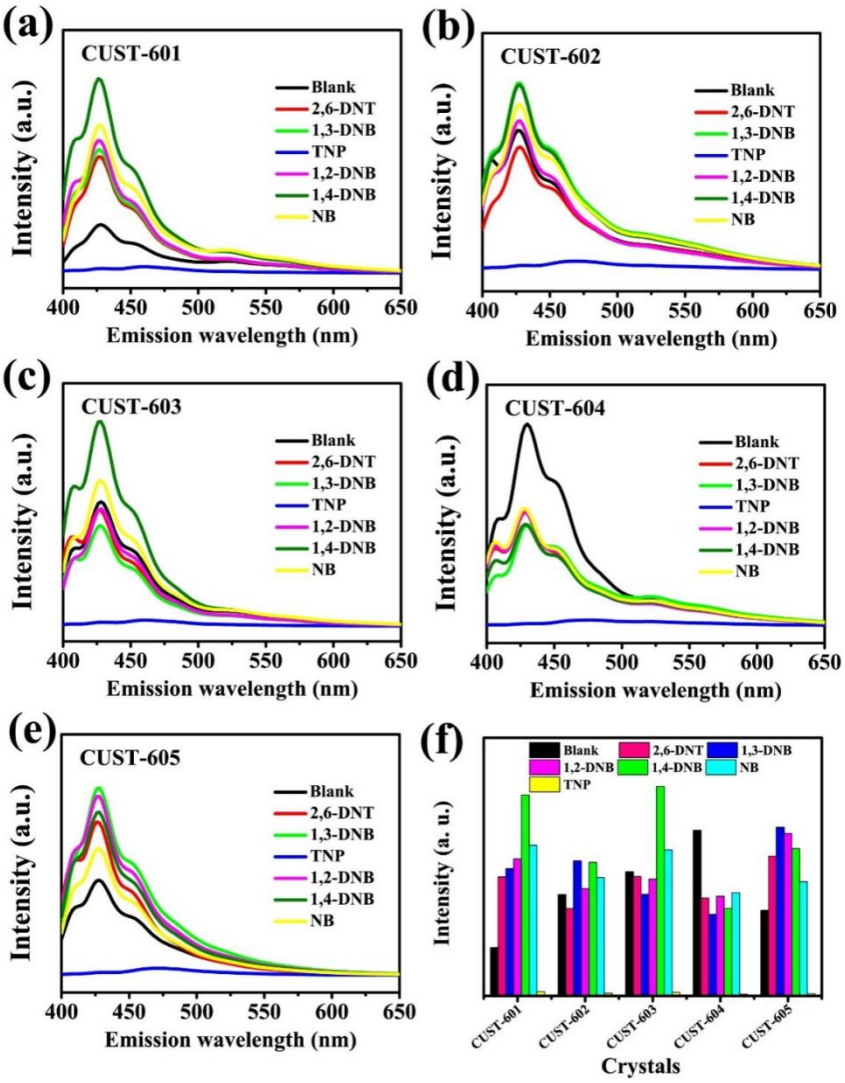

Figure S34. Fluorescence spectrums of (a) CUST-601, (b) CUST-602, (C) CUST-603, (d) CUST-604, (e) CUST-605 for detecting 2,6-DNT, 1,3-DNB, TNP, 1,2-DNB, 1,4-DNB and NB, (f) contrast of fluorescence intensity of CUST-601~605 with different NACs.

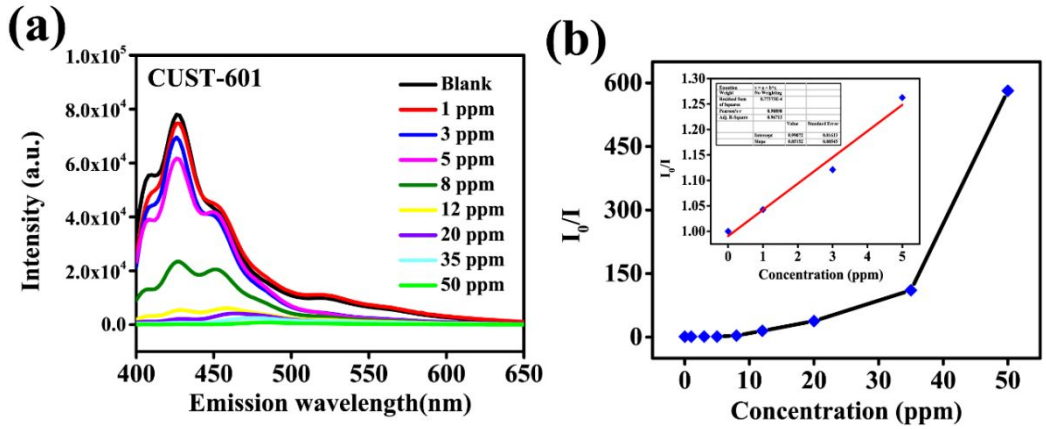

Figure S35. (a) Fluorescence spectrums of CUST-601 with increasing TNP concentration. (b) S-V plot of CUST-601 with increasing TNP concentration.

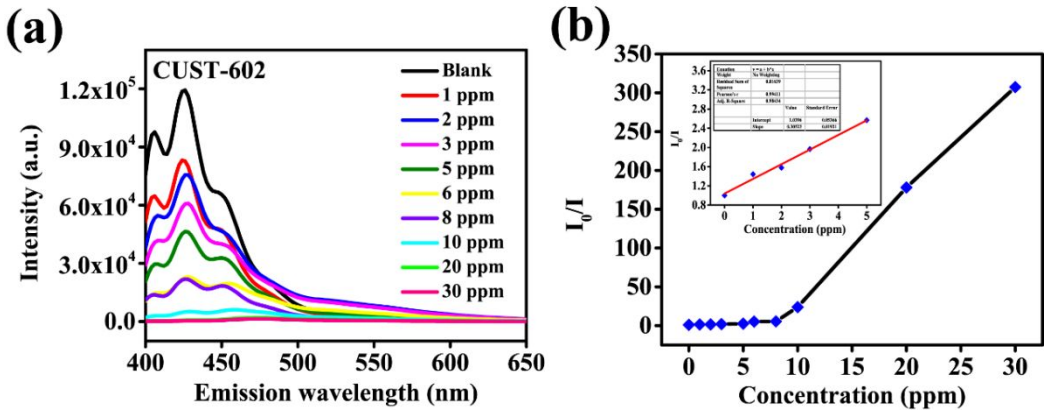

Figure S36. (a) Fluorescence spectrums of CUST-602 with increasing TNP concentration. (b) S-V plot of CUST-602 with increasing TNP concentration.

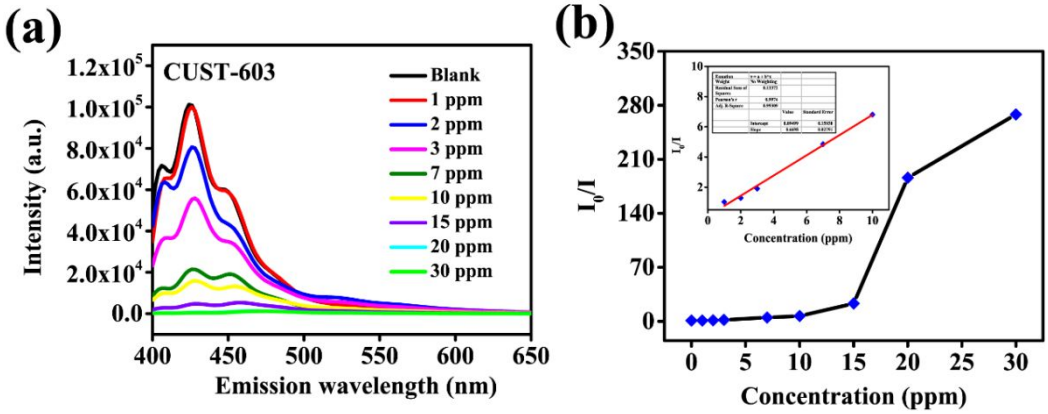

Figure S37. (a) Fluorescence spectrums of CUST-603 with increasing TNP concentration. (b) S-V plot of CUST-603 with increasing TNP concentration.

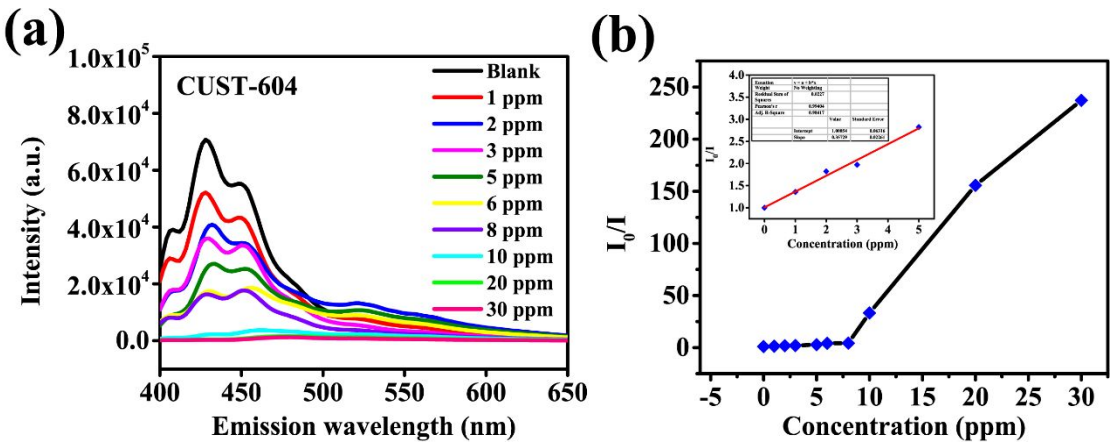

Figure S38. (a) Fluorescence spectrums of CUST-604 with increasing TNP concentration. (b) S-V plot of CUST-604 with increasing TNP concentration.

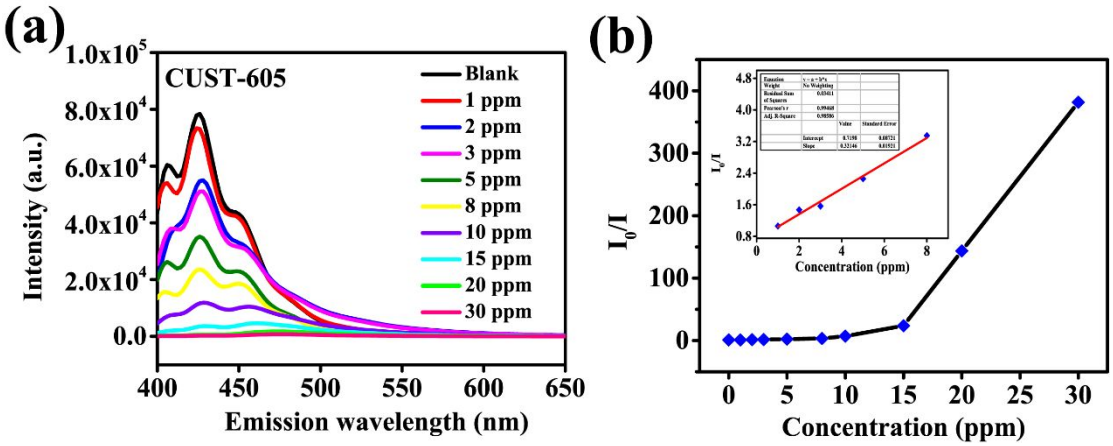

Figure S39. (a) Fluorescence spectrums of CUST-605 with increasing TNP concentration. (b) S-V plot of CUST-605 with increasing TNP concentration.

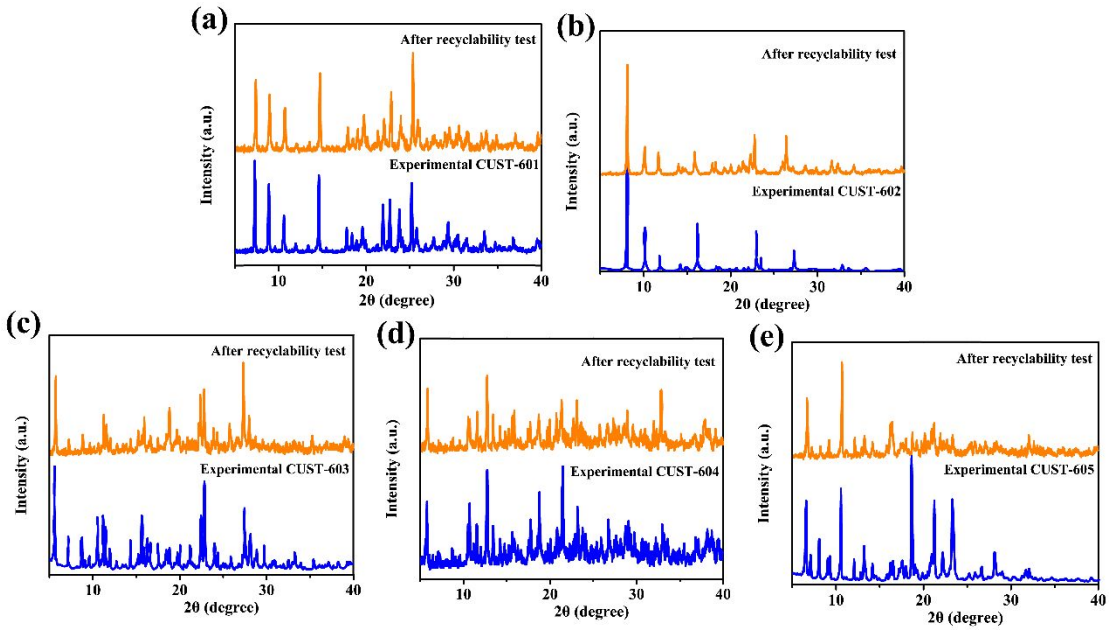

Figure S40. PXRD spectrum after recyclability test of **CUST-601 ~ 605**.

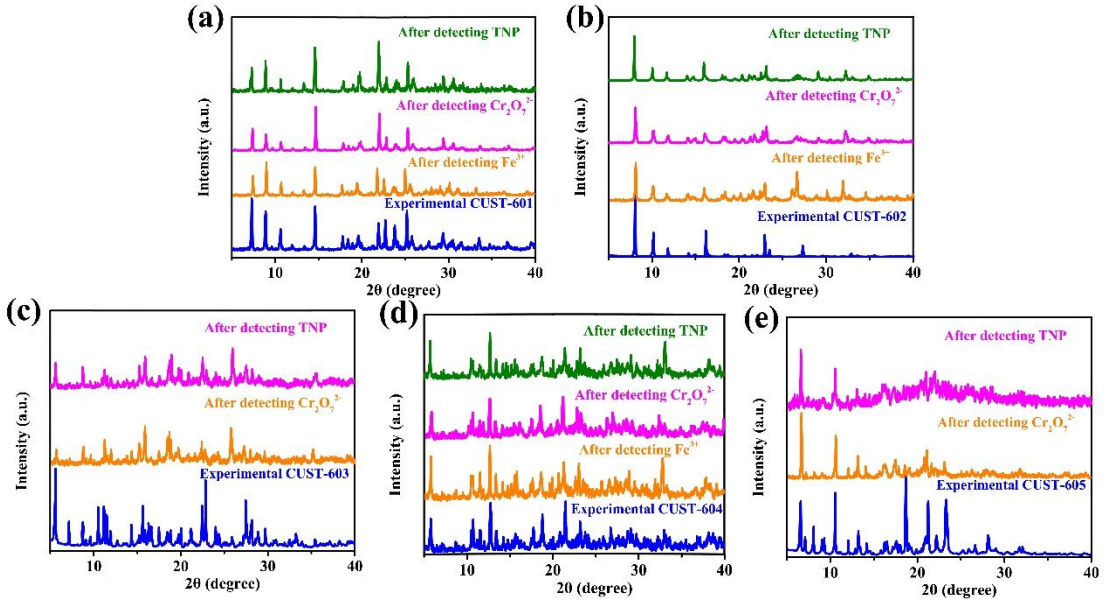

Figure S41. PXRD spectrum after anti-interference test of **CUST-601 ~ 605**.

Table S12. The Linearity range, K_{sv} and R^2 values of detecting Fe^{3+}, $Cr_2O_7^{2-}$ and TNP.

	Fe^{3+}			**$Cr_2O_7^{2-}$**			**TNP**		
Crystal	Linearity range (μM)	K_{sv} (M^{-1})	R^2	Linearity range (μM)	K_{sv} (M^{-1})	R^2	Linearity range (ppm)	K_{sv} (M^{-1})	R^2
CUST-601	0-150	2.81×10^3	0.9789	60-300	1.35×10^3	0.9826	0-5	1.18×10^4	0.9671
CUST-602	50-250	2.14×10^3	0.9767	0-250	2.15×10^3	0.9921	0-5	6.99×10^4	0.9843
CUST-603		-	-	0-300	3.26×10^3	0.9935	1-10	1.53×10^5	0.9930
CUST-604	0-100	1.57×10^3	0.9958	100-250	5.48×10^3	0.9808	0-5	8.18×10^4	0.9841
CUST-605		-	-	60-350	5.83×10^2	0.9749	1-8	7.20×10^4	0.9858

Table S13. The Linearity range, K_{sv} and R^2 values of detecting Fe^{3+}, $Cr_2O_7^{2-}$ and TNP.

MOF	**LOD**			**Ref.**
	Fe^{3+}	$Cr_2O_7^{2-}$	TNP	
CUST-601	**4.48 μM**	**10.08 μM**	**245 ppb**	**This work**
CUST-602	**5.88 μM**	**5.86 μM**	**41 ppb**	**This work**
CUST-603	**-**	**3.86 μM**	**19 ppb**	**This work**
CUST-604	**8.02 μM**	**2.29 μM**	**35 ppb**	**This work**
CUST-605	**-**	**21.6 μM**	**40 ppb**	**This work**
Zn-MOF	1.78×10^{-4}	-	-	[5]
$[Zn(NIPH)_2(HPF)_2]$	15.5 ppb	22.4 ppb	-	[6]
$Cd_3(NTB)_2(DPP)_2]\bullet3DMA\bullet H_2O$	13.6 μM	64.0 μ M	-	[7]
$[Cd_3(L)_2(Br\text{-}BDC)_6(DMF)_2]$	76.9 ppb	-	150 ppb	[8]
$[CdL_2(2,6\text{-}BIP)]\bullet DMF$	-	-	1.10×10^{-6} M	[9]
$[Cd_3(H_2O)_3(L)(tib)_2]\bullet5DMA\bullet3H_2O$	0.718 mM	-	74 μM	[10]
[Cd-1.5(L)(2)(bpy)(NO_3)]	166 ppb	114 ppb	-	[11]
$[Eu(Hpzbc)_2(NO_3)]\cdot H_2O$	2.6×10^{-5} M	2.2×10^{-5} M	-	[12]

Reference

[1] Liu, J. Y.; Wang, Q.; Zhang, L. J.; Yuan, B.; Xu, Y. Y.; Zhang, X.; Zhao, C. Y.; Wang, D.; Yuan, Y.; Wang, Y.; Ding, B.; Zhao, X. J.; Yue. M. M. Anion-Exchange and Anthracene-Encapsulation within Copper(II) and Manganese(II)-Triazole Metal-Organic Confined Space in a Single Crystal-to-Single Crystal Transformation Fashion. *Inorg. Chem.* **2014**, *53*, 5972−5985.

[2] Luo, T. T.; Tsai, H. L.; Yang, S. L.; Liu, Y. H.; Yadav, R. D.; Su, C. C.; Ueng, C. H.; Lin, L. G.; Lu, K. L. Crystal Engineering: Toward Intersecting Channels from a Neutral Network with a bcu-Type Topology. Angew. *Chem., Int. Ed.* **2005**, *44*, 6063.

[3] Wang, N.; Ma, J. G.; Shi, W.; Cheng, P. Two Novel Complexes Based on Hexagonal-Planar {Co6} and Rhombic {Zn4} Clusters with Different Eight-connected Topologies. *CrystEngComm*. **2012**, *14*, 5634.

[4] Du, Y.; Wang, X. F.; Liang, Y. F.; Ji, J. W.; Han, Z. B. A New Eight-connected CsCl-Type Topological Net Based on Trinuclear Co(II) Clusters as Nodes. *Inorg. Chem. Commun.* **2011**, *14*, 1940.

[5] Yang. H. Y.; Qi, D. Y.; Chen, Z. Z.; Cao, M. Y.; Deng, Y. J.; Liu, Z. X.; Shao, C. Y.; Yang, L. R. A Zn-based Metal–Organic Framework as Bifunctional Chemosensor for the Detection of Nitrobenzene and Fe^{3+}. *Journal of Solid State Chemistry*. **2021**, *296*, 121970.

[6] Akram, M. A.; Ye, J. W.; Wang, G. Y.; Shi, L.; Liu, Z.; Lu, H.; Zhang, S. Q.; Ning, G. L. Bifunctional Chemosensor Based on a Dye-encapsulated Metal-Organic

Framework for Highly Selective and Sensitive Detection of $Cr_2O_7^{2-}$ and Fe^{3+} ions. *Polyhedron.* **2020**, *185*, 114604.

[7] Wang, K.; Hu, X. L.; Li, X.; Su, Z. M.; Zhou, E. L. Solvent Induced Two Cd-MOFs as Luminescent Sensors for Picric acid, Fe^{3+} and $Cr_2O_7^{2-}$. *Journal of Solid State Chemistry.* **2021**, *298*, 122128.

[8] Fan, M. Y.; Yu, H. H.; Fu, P.; Su, Z. M.; Li, X.; Hu, X. L.; Gao, F. W.; Pan, Q. Q. Luminescent Cd(Ⅱ) Metal-Organic Frameworks with Anthracene Nitrogen-containing Organic Ligands as Novel Multifunctional Chemosensors for the Detection of Picric acid, Pesticides, and Ferric Ions. *Dyes and Pigments.* **2021**, *185*, 108834.

[9] Wang, D.; Hu, Z. Y.; Xu, S. S.; Li, D. D;. Zhang, Q.; Ma, W.; Zhou, H. P.; Wu, J. Y.; Tian, Y. P. Fluorescent Metal-Organic Frameworks Based on Mixed Organic Ligands: New Candidates for Highly Sensitive Detection of TNP. *Dalton Trans.* **2019**, *48*, 1900.

[10] Sun, X. Y.; Zhang, X. D.; Xu, Z. H.; Zhao, Y.; Wang, Z. L.; Sun, W.Y. A New Two-fold Interpenetrated Cd(II)-based Metal-Organic Framework as a Fluorescent Probe for Nitro-aromatic Compounds. *J coordina chem*. **2020**, *73*, 2728-2739.

[11] Singh, M.; Kumar, G.; Neogi, S. Devising Mixed-Ligand Based Robust Cd(II)-Framework From Bi-Functional Ligand for Fast Responsive Luminescent Detection of Fe^{3+} and Cr(VI) Oxo-Anions in Water With High Selectivity and Recyclability. *Front Chem*. **2021**, *9*, 651866.

[12] Li, G. P.; Liu, G.; Li, Y. Z.; Hou, L.; Wang, Y. Y.; Zhu, Z. H. Uncommon

Pyrazoyl-Carboxyl Bifunctional Ligand-Based Microporous Lanthanide Systems: Sorption and Luminescent Sensing Properties. *Inor Chem.* **2016**, *55* (8), 3952-3959.